Packet Switching Performance at 10 Gb/s Across a 4 × 4 Optical Crosspoint Switch Matrix

Ivan B. Djordjevic, Riccardo Varrazza, Mathew Hill, and Siyuan Yu

***Abstract*—Packet-switching characteristics of an integrated 4 × 4 InGaAsP–InP active vertical coupler optical cross-point switch matrix are optimized. Optical gain differences of less then 3 dB between the shortest and longest switching paths are achieved. Bit-error rate (BER) and power penalty measurements during packet routing have been carried out over the entire 4 × 4 matrix. At 10-Gb/s packet data rate less than 1-dB power penalty is found across the switch matrix, and the possibility for error-free packet routing is demonstrated with no BER floor observed.**

***Index Terms*—Bit-error rate (BER), lossless switching, optical cross-point switch (OXS) matrix, optical packet routing, optical switch fabrics.**

I. Introduction

IN ORDER to exploit the tremendous capacity provided by optical fiber, the switching functions must be implemented in optical domain. High-speed optical switching elements will play a crucial role in future highly flexible, all-optical networks in the effort of moving the packet-switching functions to the optical layer [1], [2]. To support packet data routing, optical packet-switching elements having high extinction ratios, low polarization-dependent loss, low loss, and high-scalability are highly desirable. One such optical space switch or optical cross-point switch (OXS) matrix, based on active vertical coupler (AVC) structures, has been investigated over recent years by our research team [3], [4].

This OXS matrix is fabricated in quaternary semiconductor multilayers deposited on an InP substrate. The matrix consists of two perpendicular groups of passive ridge waveguides forming the input and output waveguides (Fig. 1). Two AVCs are formed at each cross-point by having an active waveguide stacked on top of both input and output passive waveguides. A total internal reflection (TIR) mirror cuts vertically through the active waveguide and diagonally across the waveguide intersection. This allows a 90° redirection of the optical signal from the first AVC to the second one.

In ON state (with the injection current being applied), the effective refractive index of the active upper waveguide is reduced to matching that of the lower waveguide allowing strong coupling of the input signal from the passive input waveguide to the upper active waveguide in the first AVC. The signal is reflected by the TIR, and then coupled from the upper waveguide to the output waveguide in the second AVC. The injected carriers also provide signal amplification, therefore, improving the ON–OFF contrast ratio but at the same time introducing a spontaneous emission noise. In OFF state, the effective refractive index of the upper waveguide is significantly different from that of the input and the output passive waveguides, resulting in very low coupling, and the input signal is forwarded to the next switching cell along the passive waveguide. Low-crosstalk results from high absorption of any residual coupling in the active layer. More details on the OXS architecture may be found in [3], [4]. In those previous works, it has been demonstrated that the AVC switch cells can provide switching speed of ∼1.5 ns and crosstalk levels of lower than −60 dB.

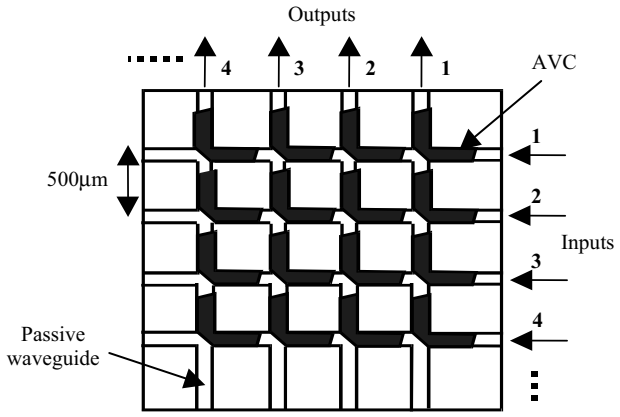

Fig. 1. Layout of the 4 × 4 cross-point switch matrix.

When designing an OXS matrix, however, a major concern is that not all signal paths are of the same length. Therefore, it is important to optimize the transmission characteristics over the entire matrix so that the quality of signals transmitted via the shortest and the longest paths in the matrix is comparable. In this letter, we describe device optimization, optical switching performance, bit-error-rate (BER) performance, and power penalties at 10-Gb/s packet data rate over the entire 4 × 4 OXS matrix.

II. 4 × 4 OXS Matrix Optimisation

The approach to achieving good performance across the matrix is to first increase individual switch cell ON-state optical gain. This can generally be achieved by maximizing the carrier-induced effective refractive index change in the active waveguide at the desired ON-state injection current density level. The passive waveguide parameters are then adjusted so that good coupling is achieved at the ON-state current level. In an AVC structure, the coupling length at which optical power maximum

Manuscript received June 23, 2003; revised August 5, 2003.

The authors are with the Department of Electrical and Electronic Engineering, University of Bristol, Bristol BS8 1TR, U.K. (e-mail: R.Varrazza @bristol.ac.uk).

Digital Object Identifier 10.1109/LPT.2003.818943

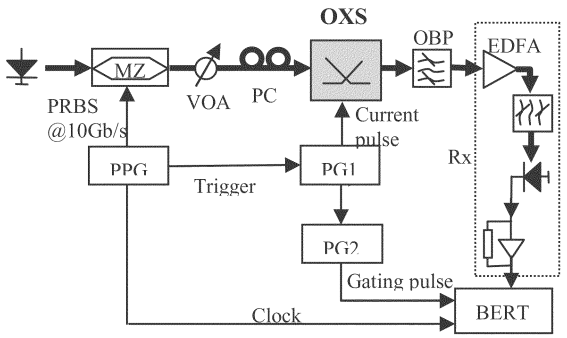

Fig. 2. BER test setup. PC: polarization controller; MZ: Mach–Zehnder modulator; Rx-receiver; PG: pulse generator; BERT: BER detector.

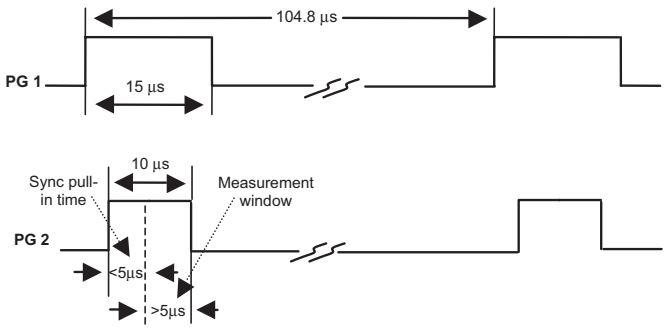

Fig. 3. Packet–burst timing diagram. PG1: switching pulses; PG2: gating pulses.

occurs in the active layer differs from a classic passive directional structure, and does not coincide with the length at which optical power minimum occur in the passive waveguide.

Apart from common reasons such as material, waveguide, and TIR mirror scattering losses, the OFF-state transmission loss is mainly caused by residual coupling of light into the active layer now in a high absorption state. To achieve transmission uniformity, the OFF-state loss of switch cells should be minimized. This is achievable by epilayer structure adjustments resulting in longer coupler lengths. However, the physical size and the total injection current–power consumption requirements limit the coupler length. A tradeoff between the AVC length and the OFF-state loss is, thus, necessary. Resulting designs do not necessarily provide maximum gain for each individual switch cell, but would result in a 4 × 4 matrix with minimized path dependent gain.

One of the several designs, aiming at an OFF-state loss of ∼0.5 dB per cell, have an intrinsic separate-confinement-heterostructure upper active waveguide with 7×75 Å unstrained InGaAs quantum-wells ($\lambda_{\mathrm{PL}} = 1560$ nm) and 60 Å Q1.3 barriers. The 0.7-μm-thick Q1.2 passive waveguide layer and the 1.35-μm-thick InP spacing layer are n-doped. The wafers are metal–organic vapor phase epitaxy grown. The switch matrices, with 5-μm ridge waveguide width and 500-μm cell size, are defined by a self-aligned two-level metal–dielectric masking scheme allowing good alignment of the TIR mirror relative to the waveguides. The structure is etched in two dry etching steps using inductive coupled plasma/reactive ion etching plasma in Cl_2–N_2 ambient achieving high smoothness and verticality of the sidewall and the TIR mirror. SiO_2 passivation and Ti–Pd–Au p-contact deposition finish the device.

III. Test Setup

The 4 × 4 OXS matrix device used in this experiment is bonded to a copper heatsink with device side up. The temperature of the heatsink is controlled at 20 °C by a thermoelectric cooler.

As shown in Fig. 2, a continuous-wave laser source operating at 1550-nm wavelength is externally modulated using a Mach–Zehnder modulator by a continuous pseudorandom binary sequence (PRBS) of length $2^{15}-1$ at bit rate 10 Gb/s from a pulse-pattern generator (PPG). The optical data passed through the polarization controller are coupled to the OXS by a fiber lens. The continuous optical data stream is chopped into packets by the switching operation of the switch cell being tested, which are driven by current pulses generated by PG1 and synchronised to a trigger pulses provided by the PPG at the start of every 32 PRBS cycles. The data packets so formed are forwarded to the corresponding output port, and again coupled into fiber by a second fiber lens. The optical bandpass (OBP) filter that follows the OXS is used to suppress the spontaneous emission noise. The OXS and fiber lenses are supported by micro-positioning stages placed on an optical bench in order to avoid disturbances caused by environmental vibration, which would result in bursts of high BER.

The 10-Gb/s burst-mode receiver consists of an erbium-doped fiber amplifier used as preamplifier, and a 12-GHz bandwidth photoreceiver with the trans-impedance amplifier output connected to the BER detector. The BER detector is operated in a burst mode, clocked by a gating pulse generated by PG2 that is slaved to PG 1, therefore, also synchronised to the PPG trigger output. The length of the BER test window is determined by this gating pulse, which is properly delayed relative to the switching pulse to avoid detecting the degraded signal during the switch-ON and switch-OFF times (which in true packet switching applications should usually coincide with guard times). The packet and BER detector gating timing and packet interval are illustrated in Fig. 3. The duration of each packet is 15 μs. The BER detector gating pulse is 10 μs wide, part of which (<5 μs) is used by the BERT to achieve synchronization, giving a BER measurement time window of >5 μs, ensuring coverage of a complete PRBS cycle of 3.276 μs. Packets are switched every 104.8 μs.

IV. Pulsed Optical Power Switching Performance

Optical power transmission characteristics across the 4 × 4 device have been investigated for transverse electric (TE) input polarization using switching current pulses shown in Fig. 3. The results for the shortest, longest, and other paths across the 4 × 4 OXS matrix are illustrated in Fig. 4, at the gain peak wavelength of the active waveguide with TE polarization. For each path, the lossless switching with optical gain up to 5 dB is found. The difference in transmission characteristics between longest and shortest paths less then 3 dB is observed at switch current of 550 mA. This meets the design requirement of 0.5 dB/cell OFF-state loss, since the longest path includes six OFF-state switching cells. For almost all cells, currents higher than 550 mA result in

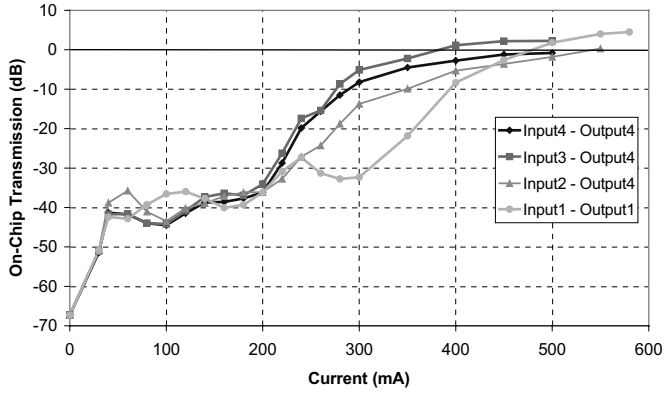

Fig. 4. Switching characteristics for shortest, longest, and across the 4 × 4 OXS matrix.

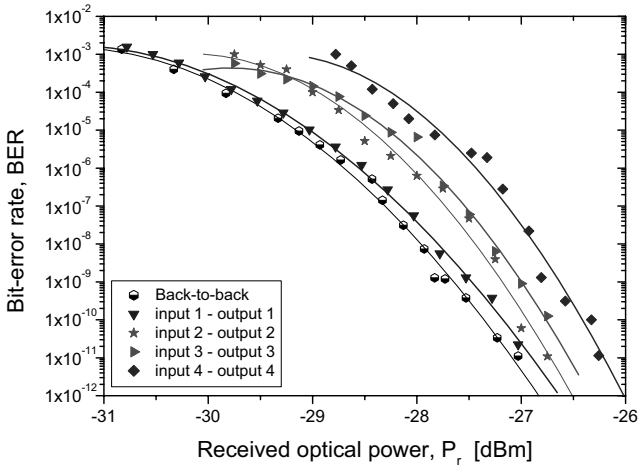

Fig. 5. Burst mode BER performance for the diagonal switching cells.

excessive Fabry–Pérot resonance due to imperfect facet antireflection. However, in some cells, higher gain is still achievable when the current is further increased.

With the device in OFF-state (zero current), the measured on-chip leakage level is as low as −67 dB between all inputs and outputs, resulting in an ON–OFF contrast of about 70 dB at 500 mA. Furthermore, no increase in leakage signal levels could be measured in all other outputs with any switch path in the ON-state, confirming the excellent crosstalk suppression in the switch matrix.

V. Packet Data Switching Performance

In Fig. 5, the burst BER performance for the switching cells along the diagonal of the matrix (i.e., Input 1–Output 1, Input 2–Output 2, etc.) is shown. At $\mathrm{BER} = 10^{-11}$, power penalties of less than 1 dB are observed for entire diagonal switching cells, with larger penalties for longer paths as expected.

In Fig. 6, the burst BER performance for the switching cells on the left-most column of the matrix (i.e., Input 4–Output 4, Input 3–Output 4, etc.) is shown. Similar to Fig. 5 at BER of 10^{-11}, power penalties less than 1 dB are observed for the entire column. The worst BER performance of the Input 2–Output

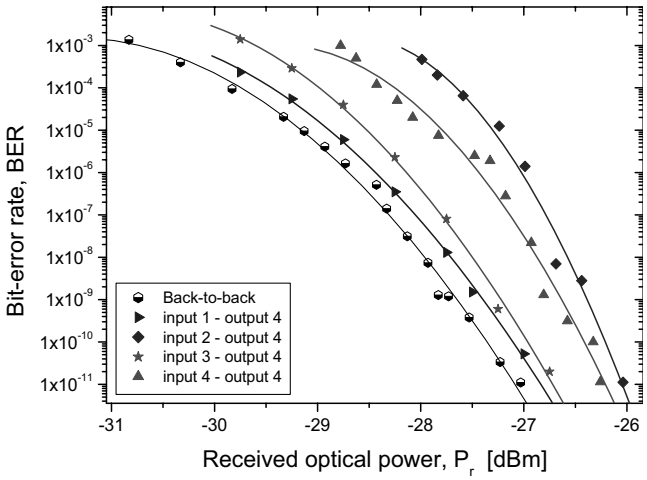

Fig. 6. Burst mode BER performance for the left-most column switching cells.

4 ports is attributed to the higher loss caused by imperfect fabrication quality, although the power penalty is kept within 1 dB.

For all cells in the matrix, error-free packet routing operation can be achieved without any BER floor.

VI. Conclusion

A compact integrated lossless 4 × 4 matrix optical switch, employing optical switching cells based on AVC technology, has been optimized on an InGaAsP–InP substrate. Lossless switching, with optical gain up to 5 dB, is achieved across the matrix. The optical power transmission characteristics difference between the shortest and the longest paths is less than 3 dB. BER and power penalty performance of the AVC 4 × 4 optical space switch matrix are fully investigated under optical packet routing operation conditions at a data rate of 10 Gb/s. Error-free operation is demonstrated for transmission through all switch cells across the entire matrix, and power penalty uniformity of less than 1 dB across the matrix has been achieved.

Since this OXS operates at high switching speeds (∼1.5 ns), demonstrates ultralow crosstalk (∼ −67 dB), very high ON–OFF contrast ratio (∼70 dB), and is very compact in size, it is a strong candidate for future high-speed highly flexible all-optical packet-switching networks. However, it should be noted that these devices are designed for TE polarization only.

References

[1] G. I. Papadimitriou, C. Papazoglou, and A. S. Pomportsis, "Optical switching: switch fabrics, techniques, and architectures," *J. Lightwave Technol.*, vol. 21, pp. 384–405, Feb. 2003.

[2] S. J. B. Yoo *et al.*, "Rapidly switching all-optical packet routing system with optical-label swapping incorporating tunable wavelength conversion and a uniform-loss cyclic frequency AWGR," *IEEE Photon. Technol. Lett.*, vol. 14, pp. 1211–1213, Aug. 2002.

[3] S. Yu, M. Owen, R. Varazza, R. V. Penty, and I. H. White, "Demonstration of high speed optical packet routing using vertical coupler crosspoint space switching array," *Electron. Lett.*, vol. 36, pp. 556–558, 2000.

[4] S. Yu, M. Owen, R. Varazza, R. W. Penty, and I. H. White, "High speed optical packet routing demonstration of a vertical coupler crosspoint space switch array," in *Proc. CLEO*, 2000, pp. 256–257.